

Annals of Medicine



ISSN: (Print) (Online) Journal homepage: www.tandfonline.com/journals/iann20

SNRPB and CEP290, predicting the prognosis of diffuse large B cell lymphoma and associated with tumour immune microenvironment

Jing Tang, Bo Lu, Ting Bin, Xiao-Jun Xu, Chao Lin, Ying Wang & Wen-Lin Xie

To cite this article: Jing Tang, Bo Lu, Ting Bin, Xiao-Jun Xu, Chao Lin, Ying Wang & Wen-Lin Xie (2024) SNRPB and CEP290, predicting the prognosis of diffuse large B cell lymphoma and associated with tumour immune microenvironment, Annals of Medicine, 56:1, 2425065, DOI: 10.1080/07853890.2024.2425065

To link to this article: https://doi.org/10.1080/07853890.2024.2425065

<u>a</u>	© 2024 The Author(s). Published by Informa UK Limited, trading as Taylor & Francis Group
+	View supplementary material 🗷
	Published online: 03 Dec 2024.
	Submit your article to this journal 🗷
hil	Article views: 195
Q	View related articles 🗹
CrossMark	View Crossmark data 🗹

ANNALS OF MEDICINE 2024, VOL. 56, NO. 1, 2425065 https://doi.org/10.1080/07853890.2024.2425065

RESEARCH ARTICLE

3 OPEN ACCESS



SNRPB and CEP290, predicting the prognosis of diffuse large B cell lymphoma and associated with tumour immune microenvironment

Jing Tanga*, Bo Lua*, Ting Bina*, Xiao-Jun Xua, Chao Linb, Ying Wanga and Wen-Lin Xiec

^aDepartment of Haematology, The Seventh Affiliated Hospital, Sun Yat-Sen University, Shenzhen, China; ^bPediatric Hematology Laboratory, Division of Hematology/Oncology, Department of Pediatrics, The Seventh Affiliated Hospital, Sun Yat-Sen University, Shenzhen, China; ^cPathological Diagnostic Center, The Seventh Affiliated Hospital, Sun Yat-Sen University, Shenzhen, China

ABSTRACT

Background: Diffuse large B-cell lymphoma (DLBCL), the most prevalent type of non-Hodgkin's lymphoma, exhibits significant correlations with efferocytosis-related molecules (ERMs) concerning invasion, metastasis, and clinical outcomes. This study aims to establish an efferocytosis-related gene signature specifically linked to DLBCL.

Methods: Key module genes linked to DLBCL were identified via weighted gene co-expression network analysis (WGCNA) in GSE32018. Univariate Cox analysis of GSE31312 revealed ERMs associated with DLBCL survival. Differential expression analysis identified differentially expressed genes (DEGs) between DLBCL subtypes and normal samples. Venn diagram analysis identified common DEGs and key module genes. A DLBCL gene signature was built by using univariate Cox and least absolute shrinkage and selection operator (LASSO) analysis. Gene functional enrichment, immune microenvironment, and immunotherapy analyses compared two risk subgroups. Prognostic gene expression was validated at the single-cell level.

Results: In the GSE32018 dataset, 1760 key module genes related to DLBCL were identified. Using GSE31312, 14 ERMs associated with DLBCL prognosis were determined. Then, an ERMs-related prognostic signature, including small nuclear ribonucleoprotein polypeptides B (SNRPB) and centrosomal protein 290 (CEP290), was established. Independent prognostic analysis showed that the RiskScore derived from this signature was a prognostic factor. Significant immune microenvironment differences were observed between two risk subgroups. Additionally, chemotherapeutic drug sensitivity results indicated the signature could predict therapeutic response. Eventually, expression of SNRPB and CEP290 was confirmed in B cells.

Conclusion: The prognostic signature comprised of SNRPB and CEP290 based on ERMs-DEGs was established, providing a theoretical basis and reference value for DLBCL research.

ARTICLE HISTORY

Received 27 March 2024 Revised 28 June 2024 Accepted 17 October 2024

KEYWORDS

Diffuse large B cell lymphoma; efferocytosis; prognostic signature; risk subgroups; tumour immune microenvironment

1. Introduction

Lymphomas are broadly classified into non-Hodgkin and Hodgkin categories [1]. Among the non-Hodgkin types, Diffuse large B cell lymphoma (DLBCL) stands out as the predominant subtype, representing about one-third of global lymphoma diagnoses [2–4]. Molecular analysis has further segmented DLBCL into three subcategories: central B cell-like (GCB-like),

activated B cell-like (ABC-like), and a minor fraction that remains unclassified [5]. While the majority of DLBCL patients show positive responses to the standard R-CHOP regimen-a combination of rituximab, cyclophosphamide, doxorubicin, vincristine, and prednisolone-sustainable remissions are rare. Consequently, the overall survival (OS) outlook for DLBCL patients remains unsatisfactory [5,6]. This underscores the urgent need for innovative

CONTACT Chao Lin line linch26@mail2.sysu.edu.cn Pediatric Hematology Laboratory, Division of Hematology/Oncology, Department of Pediatrics, The Seventh Affiliated Hospital, Sun Yat-Sen University, Shenzhen, China; Ying Wang wangying3471@163.com Department of Haematology, The Seventh Affiliated Hospital, Sun Yat-Sen University, Shenzhen, China; Wen-Lin Xie wiewlin@mail.sysu.edu.cn Pathological Diagnostic Center, The Seventh Affiliated Hospital, Sun Yat-Sen University, Shenzhen, China

*These authors contributed equally to this work.

Supplemental data for this article can be accessed online at https://doi.org/10.1080/07853890.2024.2425065.

© 2024 The Author(s). Published by Informa UK Limited, trading as Taylor & Francis Group

This is an Open Access article distributed under the terms of the Creative Commons Attribution-NonCommercial License (http://creativecommons.org/licenses/by-nc/4.0/), which permits unrestricted non-commercial use, distribution, and reproduction in any medium, provided the original work is properly cited. The terms on which this article has been published allow the posting of the Accepted Manuscript in a repository by the author(s) or with their consent.

molecular targets in DLBCL treatment and the imperative to develop novel biomarkers for improved early detection and tailored treatment.

In the tumour microenvironment, a variety of immune cells, including macrophages, dendritic cells, regulatory T cells, and both CD8+ and CD4+ T cells, engage in the process of efferocytosis to eliminate apoptotic tumour cells [7]. The efferocytosis mechanism unfolds through four sequential stages: the emission of 'call me' signals by apoptotic cells, the recognition of these dying cells by phagocytes, their direct interaction, and the eventual release of anti-inflammatory mediators [8]. While earlier studies underscored the potential of targeting molecules and pathways associated with efferocytosis in cancer therapy [9,10], other research revealed their significant relationship with malignancy invasion, metastasis, and clinical progression, emphasizing their crucial role in the outcome of cancer treatments [7]. Yet, insights into the prognostic significance and therapeutic potential of efferocytosis-related molecules (ERMs) specifically in DLBCL remain to be fully explored.

In our research, we pinpointed genes related to efferocytosis within DLBCL. By examining their prognostic significance, we explored potential biological pathways they might be involved in. This offers an analytical foundation for assessing the prognosis of DLBCL patients while shedding light on molecular shifts that occur throughout the disease's progression.

2. Materials and methods

2.1. Data source

Multiple gene expression profile datasets of DLBCL samples were collected from Gene Expression Omnibus (GEO) database (http://www.ncbi.nlm.nih.gov/). GSE32018 datasets included 22 DLBCL and 7 normal samples, while GSE31312 datasets contained 470 DLBCL samples with survival information. Additionally, single-cell RNA sequencing (scRNA-seq) data from 4 DLBCL and 4 normal tissues were retrieved from GSE182434. The prognostic model validation dataset was downloaded from The Cancer Genome Atlas (TCGA) database, which included 48 DLBCL samples with survival information. A total of 72 efferocytosis-related molecules (ERMs) were derived from reported literature [11,12].

2.2. Weighted gene co-expression network analysis (WGCNA)

The DLBCL was considered as clinical trait for WGCNA of GSE32018 datasets *via* 'WGCNA' (version 1.70-3)

package [13]. Firstly, we clustered all samples and removed outliers to ensure the accuracy of the analysis. Then, a trait heat map and sample dendrogram were constructed, and the soft threshold was determined. The similarity between genes was calculated according to the adjacency, and a phylogenetic tree of the genes was obtained. The modules were divided *via* dynamic tree cutting algorithm with a minimum module size of 100. We then classified the genes into different modules by dynamic tree cutting algorithm. The module dissimilarity threshold (MEDissThres) was set to 0.2 to merge the similar modules. Finally, the modules with the highest correlation to DLBCL were used as key modules for subsequent analysis.

2.3. Consensus clustering analysis and assessment

In this study, GSE31312 was applied as the training set. Univariate COX analysis was utilized to screen ERMs associated with DLBCL patient survival. With the assistance of the 'ConsensusClusterPlus' package (version 1.62.0) [14], 470 DLBCL samples were clustered based on the expression of ERMs linked to patient survival. By excluding samples without survival data, we carried out a Kaplan-Meier (K-M) survival analysis based on different clustering subtypes. To examine the heterogeneity among different subtypes, a principal component analysis (PCA) was implemented using 'stats' package (version 0.12.1). Meanwhile, ERMs linked to DLBCL patient survival were analyzed between different subtypes using 'ggpubr' package (version 0.4.0). With reference to the LM22 gene set, the CIBERSORT algorithm (version 1.03) was applied to calculate the proportion of 22 immune cells in all tumour samples. The expression levels of 23 immune checkpoints [15] were compared across different subtypes using the rank-sum test.

2.4. Differential analysis

In GSE31312, the 'limma' package (version 1.36.0) [16] was executed to obtain the differentially expressed genes1 (DEGs1) between different clustering subtypes, using adj.p<0.05 and $|log_2FC| > 0.5$ as the threshold. Gene Ontology (GO) enrichment and Kyoto Encyclopaedia of Genes and Genomes (KEGG) enrichment analyses of DEGs1 was conducted *via* 'clusterProfiler' package (version 4.4.4) [17], adopting adj.p<0.05 as the criteria. The same method was utilized to obtain DEGs2 between DLBCL and normal groups in GSE32018 datasets. Volcano plot and heat map were applied to illustrate DEGs. The intersection of DEGs1, DEGs2, and key module genes associated with DLBCL were determined using a Venn diagram.

2.5. Risk score-based subgroup analysis of DLBCL patients

Univariate cox and least absolute selection and shrinkage operator (LASSO) regression analyses were vielded to screen prognostic ERMs in GSE31312 datasets. The risk score model calculating formula was: risk score = $\sum_{i=1}^{n}$ (coefficient(genei)*expr(genei)). Based on median value of risk score from each sample, DLBCL patients with survival information were categorized into two risk subgroups (low-risk and high-risk). The prognostic reliability of the model was assessed by K-M curves and receiver operating characteristic (ROC) curves for 1-, 2-, and 3-year intervals. Simultaneously, TCGA-DLBCL datasets was regarded as an external verification set for the risk model.

2.6. Clinical nomogram model

For the construction of the clinical nomogram model, the risk score, sub-type (GCB), age, gender, Ann Arbor stage (AAS), ECOG performance status, International Prognostic Index (IPI) score, presence of bulky disease (Bulky code), and lactate dehydrogenase (LDH) levels were enrolled into univariate and multivariate Cox regression analyses to authenticate independent prognostic predictors. A nomogram incorporating independent factors was developed to predict 1-, 2-, and 3-year survival probability of DLBCL patients. The predictive accuracy of the nomogram was evaluated using calibration curves and ROC curves.

2.7. Gene set enrichment analysis (GSEA)

The 'limma' package [18] was utilized to calculate the log₂FC between two risk subgroups. Then, based on GO (biological process) and KEGG gene set, GSEA (adj.p < 0.05) was performed for find related pathways between two risk groups.

2.8. Immune feature estimation and therapy analysis

Leverage LM22 gene set, the CIBERSORT algorithm was yielded to calculate the expression of 22 immune cells in DLBCL microenvironment. Subsequently, correlation coefficients between differential immune cells and prognostic genes associated with ERMs were analyzed. The 'estimate' package was applied to obtain and compare the Immune score, Stromal score and ESTIMATE score of tumour tissues. Meanwhile, in order to study the immune status of DLBCL, differences in 11 immune checkpoint genes between the high- and low-risk groups were compared [19]. The Spearman method was used to analyze the correlations between risk score and immune checkpoint genes. Additionally, the TIDE score, Dysfunction score, Exclusion score, CD8, and CD274 were compared between the highand low-risk groups. The correlation between risk score and the inhibitory concentration (IC₅₀) of 138 drugs was analyzed using 'pRRophetic' package (version 0.5).

2.9. Construction of competing endogenous RNA (ceRNA) network

The miRNAs associated with prognostic genes were predicted through miRWalk database (http://mirwalk.umm. uni-heidelberg.de/), with screening criteria of energy < -15 and bindingp = 1. The lncRNAs associated with miRNAs were predicted using Starbase database (https:// starbase.sysu.edu.cn/index.php), with screening criteria of clipExpNum > 1 and geneType=lincRNA. Moreover, the 'IncRNA-mRNA-miRNA' network was constructed via Cytoscape software (version 3.8.2) [20].

2.10. ScRNA-seg analysis

Firstly, scRNA-seq data was filtered using R package 'Seurat' (version 5.0.1) [21] in GSE182434. The 'PercentageFeatureSet' function was used to calculate the mitochondrial genes, and cells with fewer than 10% mitochondrial genes were retained. Subsequently, the Find Variable Features function in the R package 'Seurat' was used to screen out the top 2000 highly variable genes for downstream analysis. Principal component analysis (PCA) was then conducted to reduce dimensionality. Next, FindNeighbors and FindClusters functions were used for unsupervised clustering analysis of cells. We then used Uniform Manifold Approximation and Projection (UMAP) to display the results of the clustering. The marker genes of each cell cluster were compared with the marker genes of each cell type in the CellMarker database to determine the type of cell subgroup type. The R package 'SingleR' (version 2.0.0) was deployed to helping annotate cell types. Following this, the expression of prognostic genes in different cell types was analyzed by plotting UMAP maps and violin plots. Monocle3 (version 2.14.0) [22] was used for cell trajectory analysis and 'CellPhoneDB' was used for cell communication analysis.

2.11. Immunohistochemistry

In this study, sample tissues were obtained from tumour tissues of patients with diffuse large B cell

lymphoma (DLBCL), and normal lymph nodes that were not invaded by the tumour. Approval from the hospital ethics committee and informed consent from the patients were obtained. During the procedure, the resected tumour tissue and adjacent normal lymph nodes were initially assessed by the pathologist to ensure the representativeness and quality of the samples. The samples were then rapidly separated and labelled separately to avoid confusion. To maximise the retention of biological information in the tissues, samples were placed in collection tubes containing RNA stabiliser immediately after collection and rapidly frozen for processing. They were first snap-frozen in liquid nitrogen and then transferred to a -80°C ultra-low temperature refrigerator for long-term storage. The entire sample collection process lasted from May 2023 to April 2024, during which time the steps described above were rigorously carried out to ensure sample consistency and study reproducibility. Tumour paraffin sections were immunostained with antibodies against CEP290 (polyclonal, 1:100, Proteintech) and SNRPB (polyclona, 1:200; Proteintech) using standard protocols. Ready-touse two-step abiotin immunohistochemical assay kit (PV9000; Zhongshan Golden Bridge) was used to detect CEP290 and SNRPB in tissues. Clinical information of patients and healthy control in Supplementary Table 1. This study was approved by Ethics Committee Affiliated Hospital, Seventh Sun Yat-Sen University(KY-2024-063-01).

2.12. Statistical analysis

All analyses were executed in R software (version 4.2.2). K-M the log-rank test were used to evaluate the associations with survival time. P value < 0.05 was considered statistically significant.

3. Results

3.1. Identification of key module genes related to DLBCL in GSE32018

To seek out key modules related to DLBCL, we conducted the WGCNA. The results of sample clustering indicated that there were no outlier samples (Supplementary Figure 1). The optimal soft threshold was determined to be 5. When the mean connectivity tended to zero, the ordinate of the scale-free fit index approached the threshold value of 0.85, indicated by the red line (Figure 1A). A total of 11 modules were identified using the dynamic tree cut algorithm and by merging modules (Figure 1B). The MEred (Cor =

0.83) and MEpurple (Cor=-0.75) modules were markedly correlated with patient/control (Figure 1C), leading to the identification of 1,760 key module genes associated with DLBCL for subsequent analyses (Figure 1D).

3.2. The ERMs associated with prognosis in DLBCL

Regarding the ERMs associated with the prognosis in DLBCL, 14 ERMs were identified through univariate Cox regression analysis as being related to DLBCL prognosis (Figure 2A). We divided 470 DLBCL patients from the GSE31312 dataset into two subtypes: Cluster 1 (312 samples) and Cluster 2 (158 samples), based on the expression of ERMs linked to DLBCL prognosis (Figure 2B-C). K-M analysis revealed a significant survival difference between the two subtypes, with Cluster 1 exhibiting poorer OS (Figure 2D). PCA also demonstrated heterogeneity between the two subtypes (Figure 2E). Notably, the expression of 11 ERMs associated with DLBCL prognosis differed significantly between the two subgroups (Figure 2F). There were significant differences in the abundances of 8 immune cell types, including memory B cells, CD8 T cells, CD4 naive T cells, activated CD4 memory T cells, resting NK cells, M1 Macrophages, M2 Macrophages, and neutrophils (Supplementary Figure 2A). Additionally, 14 immune checkpoint genes, encompassing CD244, CD96, CSF1R, CTLA4, HAVCR2, IDO1, KDR, KIR2DL1, KIR2DL3, LAG3, PDCD1LG2, TGFB1, TGFBR1, and TIGIT, were significantly differentially expressed between the two subtypes (Supplementary Figure 2B).

3.3. Screening of candidate genes associated with ERMs in DLBCL

Totally 255 DEGs1 were identified in GSE31312 database, comprising 101 significantly up-regulated and 154 significantly down-regulated genes in cluster 1 (Figure 3A-B). To understand the biological significance of DEGs1, we performed functional enrichment analysis. The GO analysis revealed that these DEGs were mainly involved in the 'regulation of peroxisome proliferator activated receptor (PPAR) signalling pathway' and 'dystrophin-associated glycoprotein complex' (Figure 3C). The PPAR signalling pathway plays a crucial role in lipid metabolism and energy homeostasis, processes known to be dysregulated in cancer, including DLBCL [23]. The dystrophin-associated glycoprotein complex is significant in maintaining cellular integrity, and its disruption may contribute to the oncogenic

Figure 1. Identification of key module genes for diffuse large B-cell lymphoma (DLBCL) by weighted gene co-expression network analysis (WGCNA). (A) Selection of the optimal soft-thresholding (power). (B) Hierarchical clustering of genes and module identification. (C) Heatmap of the relationships between gene modules and differential immune cells. (D) Scatter plots of correlation between module genes and clinical traits (DLBCL and normal).

processes in DLBCL [24]. Moreover, KEGG pathway analysis suggested that DEGs1 were mainly enriched in 'Aldosterone synthesis and secretion' as well as 'Mineral absorption' (Figure 3D). Aldosterone synthesis and secretion are linked to cellular growth and immune response, which are critical aspects of DLBCL pathophysiology [25]. And the mineral absorption pathway is crucial for maintaining cellular ionic balance and metabolic functions, when dysregulated, can contribute to cancer development and progression [26]. In summary, these DEGs1 are potentially critical in understanding the microenvironmental interactions and extracellular signalling pathways that contribute to DLBCL pathogenesis. Similarly, from the GSE32018 database, we identified 2,994 DEGs2, with 1,803 significantly up-regulated 1,191 significantly and

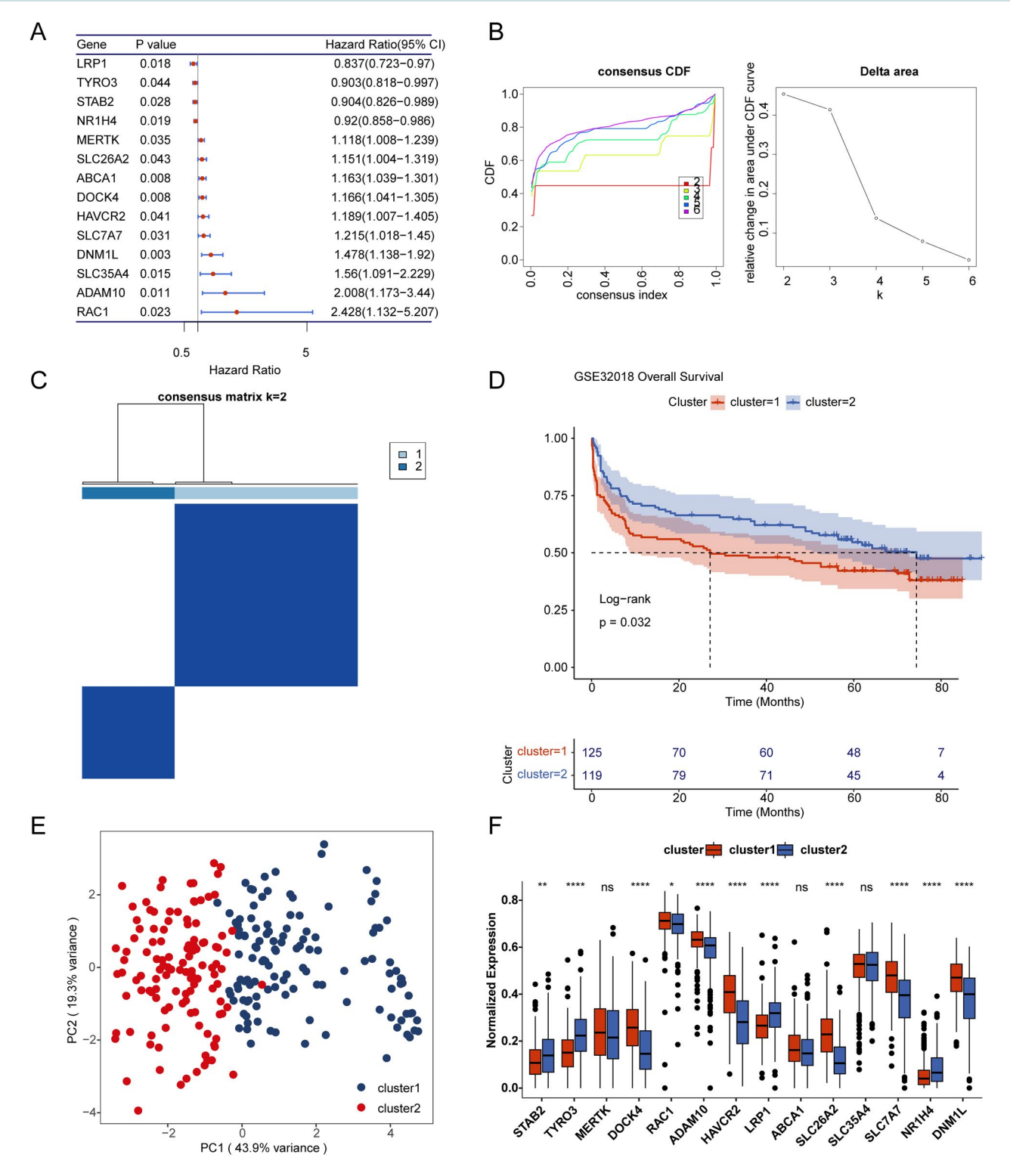


Figure 2. Identification of prognosis-related genes by consensus clustering analysis. (A) The efferocytosis-related molecules (ERMs) related to prognosis were acquired by univariate Cox regression analysis. (B) Consensus clustering CDF for k=2 to k=6 (left). The corresponding relative change in area under the cumulative distribution function (CDF) curves when cluster number changed from k to k+1 (right). The range of k changed from 2 to 6 and the optimal k=2. (C) Consensus clustering matrix of DLBCL samples for k=2. (D) The Kaplan-Meier (KM) survival curves of cluster 1 and cluster 2. (E) The principal component analysis (PCA) analysis of two clusters. (F) The expression of ERMs in two clusters. ns, not significant; *p<0.05; ***p<0.01; *****p<0.0001.

down-regulated genes in DLBCL samples (Figure 3E-F). Hence, 9 candidate genes associated with ERMs in DLBCL were obtained by overlapping DEGs1, DEGs2 and key module genes related to DLBCL (Figure 3G).

3.4. Prognostic signature based on ERMs associated with survival

Univariate regression analysis identified 2 significant genes (HR \neq 1 & p<0.05) in the GSE31312 dataset,

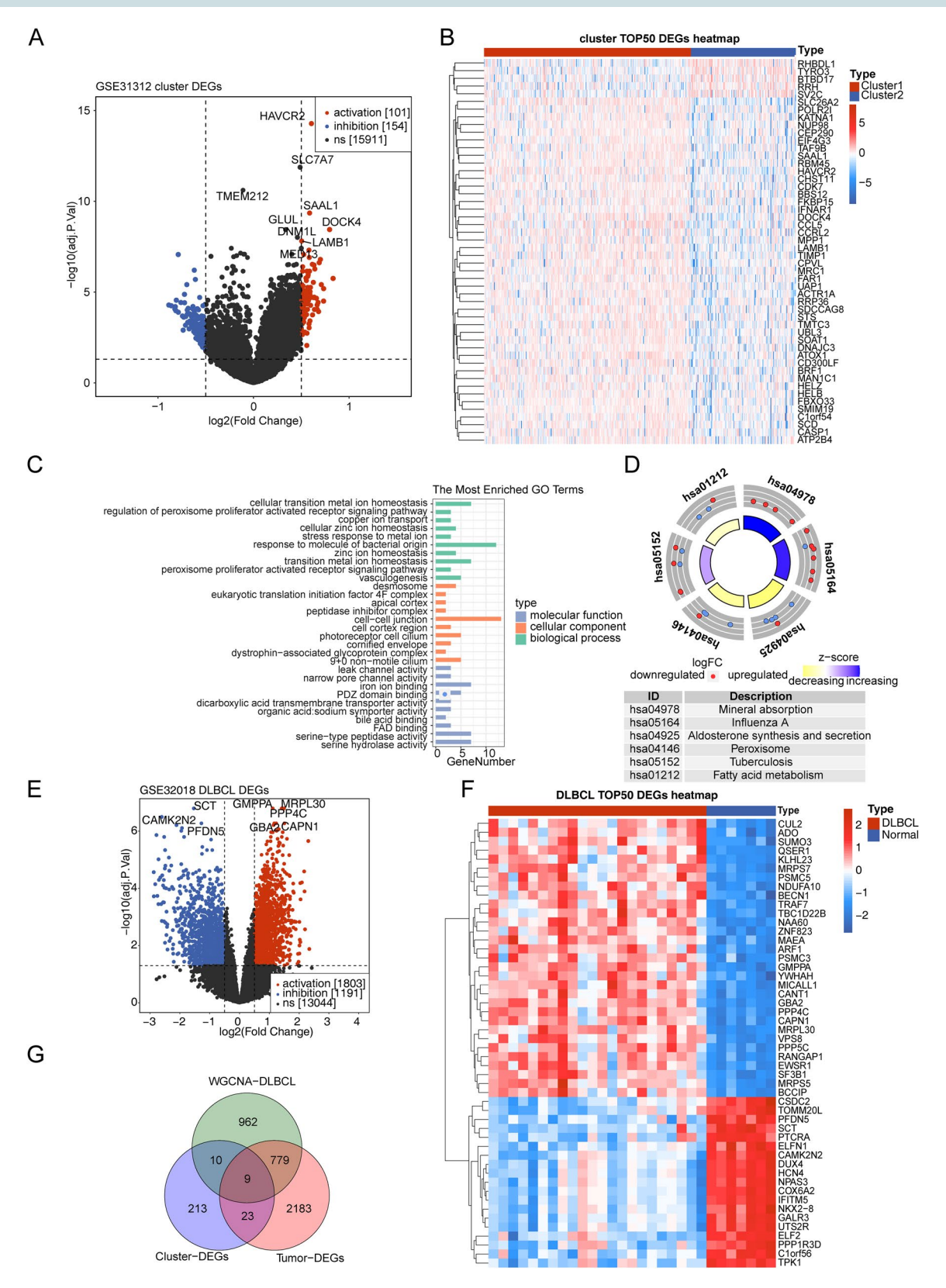


Figure 3. Identification of candidate genes for DLBCL. (A) The volcano map of differentially expressed genes (DEGs) between cluster 1 and cluster 2 in the GSE31312 database. (B) The heat map of top50 DEGs in the GSE31312 database. (C, D) The Gene ontology (GO) terms (C) and Kyoto Encyclopaedia of Genes and Genomes (KEGG) pathways (D) enriched in DEGs. (E) The volcano map of DEGs between DLBCL and normal samples in the GSE32018 dataset. (F) The heat map of top50 DEGs in the GSE32018 dataset. (G) The Venn diagram of 9 candidate genes.

namely SNRPB and CEP290 (Figure 4A). To further dig out the prognostic genes, LASSO regression analysis was conducted on 2 significant genes to unearth the optima (Figure 4B-C). Ultimately, SNRPB and CEP290 were selected as prognostic genes for building a ERMs-related prognostic signature with DLBCL. Then, DLBCL patients were divided into two risk groups (Figure 4D). High expression of 2 prognostic genes were centred on the high-risk group. Notably, we found significant survival differences between two risk groups and patients in the high-risk DLBCL group had poor survival rates (Figure 4E). To further evaluate the reliability of the model, the AUC value of the model in forecasting 1-, 2-, 3-year survival of LUAD patients was 0.60, 0.65, and 0.63 in GSE31312 datasets, indicating the risk model could forecast the survival status of DLBCL patients (Figure 4F). Next, we further validated the risk model in the external validation datasets (TCGA-DLBCL). Consistent with the results detected based on GSE31312 datasets (Figure 4G), as anticipated, patients with high-risk DLBCL exhibited poorer OS (Figure 4H). AUC values of the 1-, 2- and 3-year were basically greater than 0.60 (Figure 4I). These results showed that novel ERMs-related gene signature exhibited satisfactory predicting performance in the validation cohort.

3.5. Independent prognostic analysis for DLBCL patients

The results of Cox analyses suggested that RiskScore was prognostic independent factors (p < 0.05) (Figure 5A-B). The nomogram containing 1-, 2-, 3-year survival rates was generated (Figure 5C). The calibration and ROC curves proved that the feasibility of the nomogram was effective (Figure 5D-E).

3.6. Differential gene enrichment analysis in risk subgroups

We performed GSEA analysis in risk subgroups. GO results demonstrated that 'ribonucleoprotein complex biogenesis' was enriched in high-risk groups and 'adenylate cyclase-modulating G protein-coupled receptor signalling' was enriched in low-risk groups (Figure 6A-B). KEGG results demonstrated that 'Cell cycle' was enriched in high-risk groups and 'Cytokine-cytokine receptor interaction' was enriched in low-risk groups (Figure 6C-D).

3.7. Immune infiltration analysis

To explore the immune microenvironment of DLBCL, we analyzed the expression of 22 immune cells between two sample groups in GSE31312 (Supplementary Figure 3A). There were 12 immune cell

abundances that differed significantly in two risk-subgroups, including naive B cells, memory B cells, CD8 T cells, naive CD4 T cells, activated memory CD4 T cells, regulatory T cells, gamma delta T cells, resting NK cells, Monocytes, Macrophages M1, Macrophages M2, and Neutrophils (Supplementary Figure 3B). The correlation analysis revealed that SNRPB was positively associated with naive B cells. CEP290 was positively associated with gamma delta T cells (Figure 7A). We found that the stromal score was significantly higher in the low-risk group, while the immune score was significantly higher in the high-risk group (Figure 7B). There were 3 significantly differentially expressed immune checkpoint genes, including CD276, CD80, and TNFSF4 (Figure 7C). We also found that there were certain positive correlations between the risk score and the 9 immune checkpoints (PVR, HAVCR2, CD86, CD80, CD47, CD276, CD244, CD226 and CD160) (Supplementary Figure 3C). It was found that markers of immune exclusion, immune dysfunction, and CD274 were significant in both high- and low-risk group (Figure 7D). In order to discover potential drugs, we compared IC₅₀ of 138 drugs between all samples. There was a significant correlation between the risk score and the 27 drugs (p < 0.05) (Figure 7E). Significant differences in sensitivity to 27 drugs were observed between high- and low-risk groups (Figure 7F).

3.8. The ceRNA network analysis

The relevance of this ceRNA network analysis lies in its potential to elucidate the post-transcriptional regulatory interactions that affect SNRPB and CEP290, both of which are critical to the pathology of the disease under investigation. Therefore, to explore the regulatory mechanisms of SNRPB and CEP290, we constructed a 'IncRNA-mRNA-miRNA' network consisting of 44 IncRNAs, 7 miRNAs, and 2 mRNAs. This network comprised 53 nodes and 69 edges, illustrating the complex interactions between these RNA molecules. Notably, SNRPB was associated with hsa-miR-513a-5p, while hsa-miR-629-5p influenced the expression of CEP290 (Figure 8). This insight into the RNA-based regulatory landscape provides a foundation for further functional studies and highlights potential avenues for targeted therapeutic intervention.

3.9. Expression analysis of prognostic genes in different cells

In order to further analyze the expression and regulation of prognostic genes at the single-cell level, we

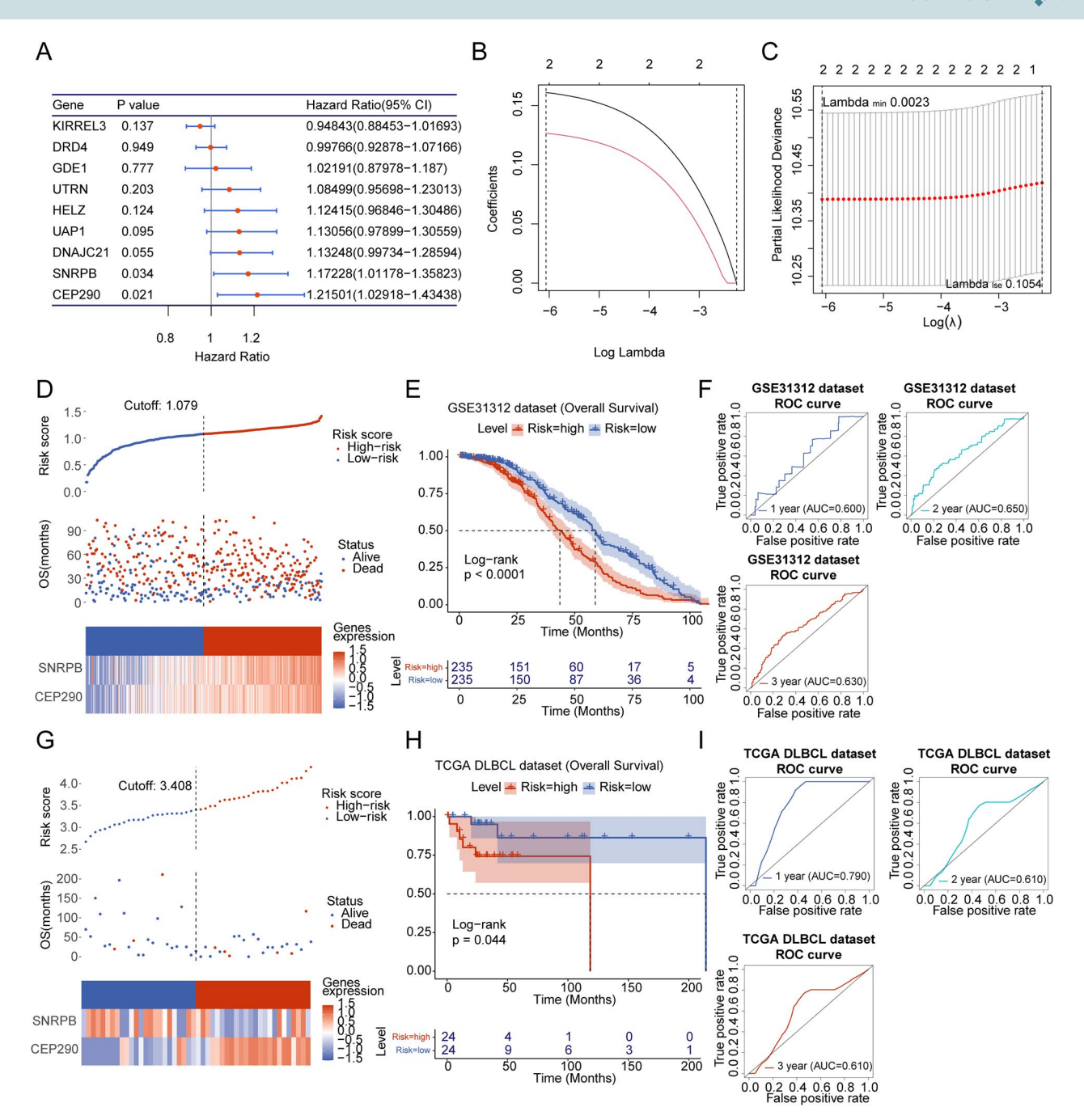


Figure 4. Establishment of prognostic signature for DLBCL. (A) Two prognostic genes obtained by univariate Cox regression analysis. (B, C) The plot of gene coefficients (B) and error plots for 10-fold cross-validation (C) in least absolute shrinkage and selection operator (LASSO) analysis. (D) The risk curve, survival state distribution, and the expression of prognostic genes. (E) The KM survival curves of high- and low-risk groups. (F) The receiver operating characteristic (ROC) curves of the prognostic signature with 1, 2, 3 years as survival time points. AUC, area under the curve. (G) The risk curve, survival state distribution, and the expression of prognostic genes in the TCGA-DLBCL dataset (validation set). (H) The KM survival curves of two risk groups in the TCGA-DLBCL dataset. (I) The ROC curves of prognostic signature in the TCGA-DLBCL dataset.

applied the GSE182434 datasets for analysis after cell filtration (Supplementary Figure 4A). In total, 2000 highly variable genes were identified (Supplementary Figure 4B). PCA plots revealed that P-values of 30 PCs were extremely significant (Supplementary Figure 4C). Consequently, we selected these 30 PCs

subsequent analyses, and the cells were classified into 11 clusters (Figure 9A) and were annotated as NK cells, Monocyte/Macrophage, B cells, and T cells (Figure 9B-C). Supplementary Figure 4D showed the distribution of 4 cell subsets in both normal and DLBCL groups. UMAP and violin diagrams revealed that the

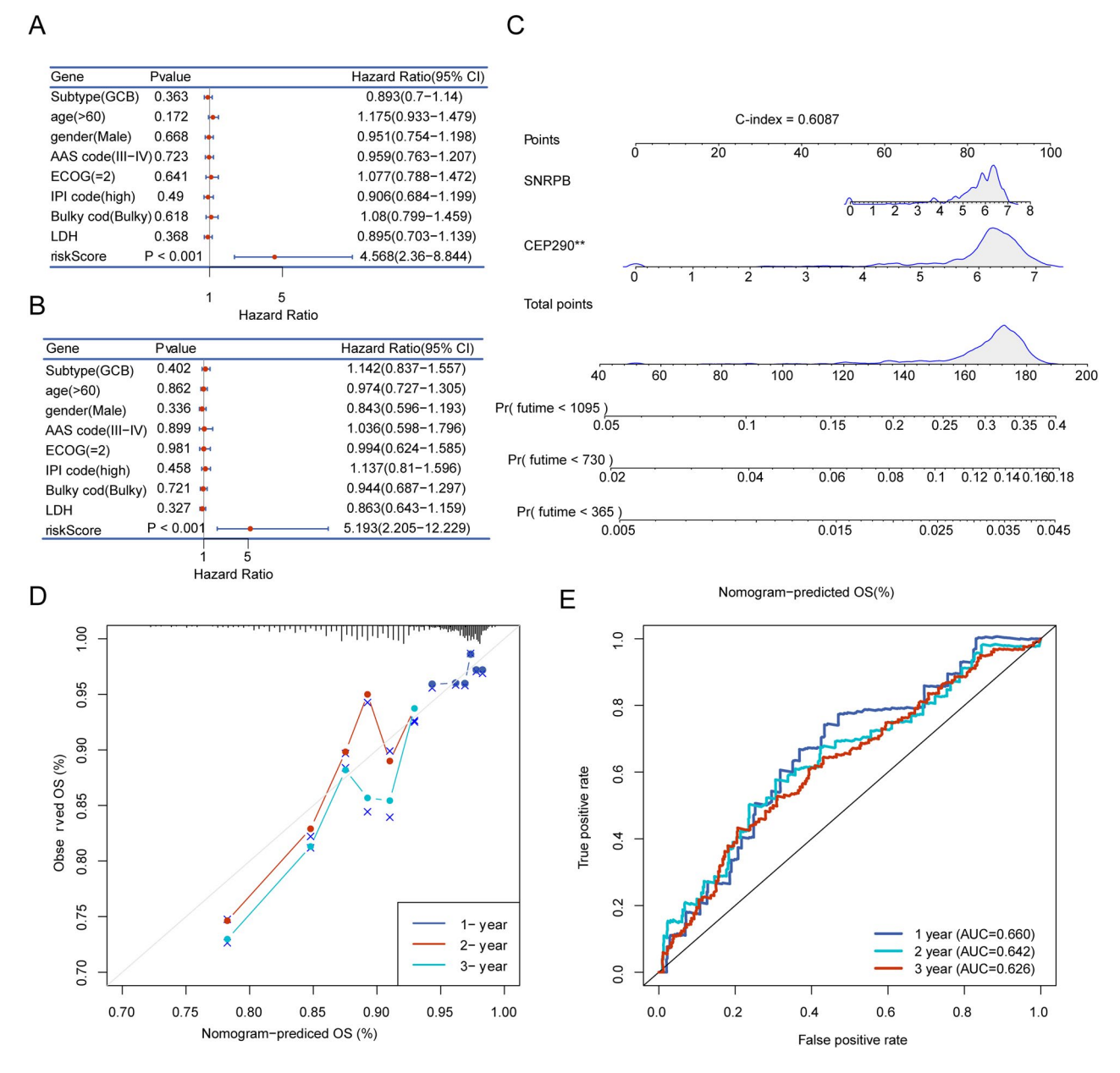


Figure 5. Independent prognostic analysis and the creation of nomogram. (A, B) The results of univariate (A) and multivariate Cox (B) Cox independent prognostic analysis. (C) The nomogram constructed based on two prognostic genes. (D) The calibration curve of the nomogram. (E) The ROC curves of the nomogram with 1, 2, 3 years as survival time points.

prognostic genes were expressed in B cells, and the expression levels of 2 prognostic genes in B cells from the DLBCL samples were lower than those in B cells from the normal samples (Figure 9D-E). Cell communication analysis identified strong interactions between key cells, with the highest number of receptor-ligand pairs occurring between monocytes/macrophages and NK cells (Supplementary Figure 5A). This finding was further corroborated by receptor-ligand interaction analysis (Supplementary Figure 5B). Using Monocle 2 for pseudotime analysis, we discovered that B cells diverged into 2 branches, possibly representing transformation trajectories from normal to malignant cells,

and it appeared that B cell differentiation in the disease group occurred earlier (Figure 9F-H). The dynamic expression profiles of 2 prognostic genes across 5 states were depicted in Figure 9I. We found that the expression of SNRPB affected the state of B cells.

3.10. Analysis of prognostic gene expression at protein level

Immunohistochemical results were summarized in Figure 10A-B. We observed that CEP290 and SNRPB proteins were more highly expressed in the tumour group compared to the normal group.

Figure 6. Gene set enrichment analysis (GSEA) enrichment analysis. (A, B) The top10 GO pathways enriched in low-risk (A) and high-risk (B) groups. (C, D) The top10 KEGG pathways enriched in low-risk (C) and high-risk (D) groups.

4. Discussion

From our understanding, advancements in DLBCL treatments have particularly been pronounced for patients undergoing subsequent therapeutic lines. Although emerging therapeutic avenues address relapsed/refractory cases of DLBCL, challenges persist for patients in advanced therapy stages [27]. Efferocytosis, crucial for tissue equilibrium, involves the non-inflammatory

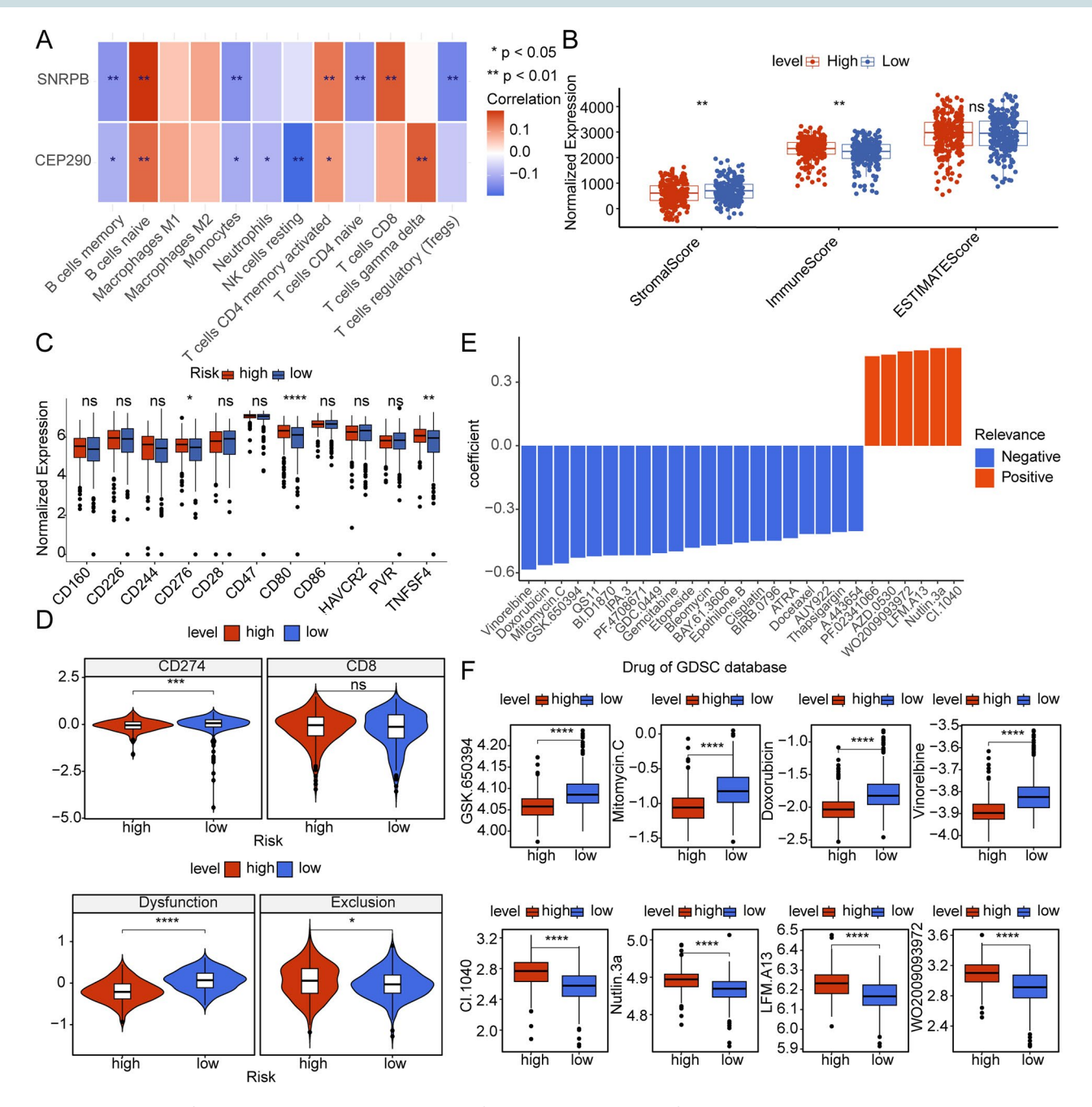


Figure 7. Immune infiltration analysis. (A) The relevance of prognostic genes to differential immune cells. *p<0.05; ** p<0.01. (B) The discrepancies of stromal score, immune score, and ESTIMATE score in high- and low-risk groups. ns, not significant; ** p<0.01. (C) The expression of immune checkpoint genes in two risk groups. ns, not significant; *p<0.05; ** p<0.01; ****p<0.001. (D) Comparison of CD274, CD8, Dysfunction, and Exclusion in the high- and low-risk groups.ns, not significant; *p<0.05; ***p<0.001; ****p<0.0001. (E) The relevance of risk score to drugs. (F) Differences in drug sensitivity between high- and low-risk groups. ****p<0.0001.

clearance of apoptotic cells, curbing undesired inflammatory reactions and avert autoimmune disturbances [28]. Amir Tajbakhsh and colleagues identified soluble receptors/ligands tied to efferocytosis, revealing both their clinical relevance and potential as diagnostic and prognostic tools [29]. Yet, insights into ERMs' prognostic and therapeutic potential in DLBCL remain scarce. Motivated by this, we crafted a gene signature focusing on efferocytosis in relation to DLBCL.

Produced by the SNRPB gene, Small nuclear ribonucleoprotein polypeptides B and B1 are common nuclear components of snRNPs, specifically U1, U2, U4/U6, and U5 [30]. These particles contribute to pre-mRNA splicing, suggesting the protein encoded by SNRPB might influence snRNP structure or the splicing process. In various tumours, there's a link between SNRPB, immune cell infiltration, and immunomodulation gene expression [30]. Notably, local studies highlighted

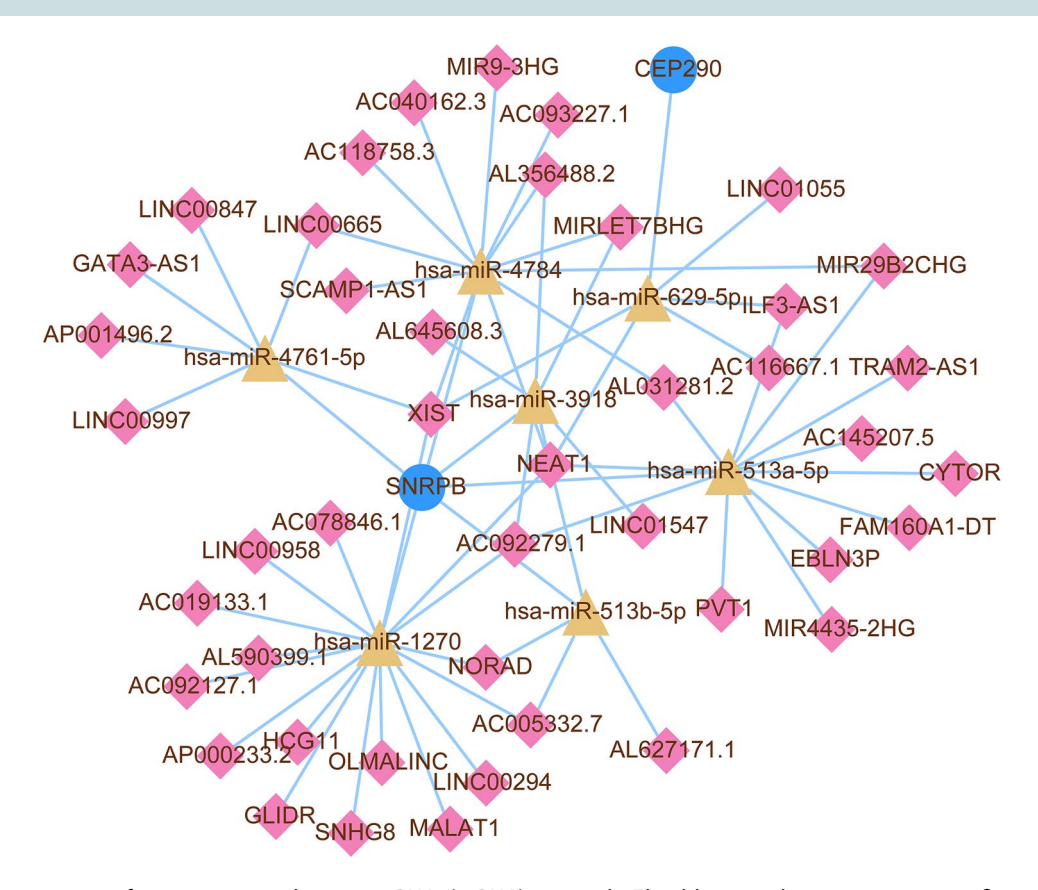


Figure 8. Construction of competing endogenous RNA (ceRNA) network. The blue graphic represents significant gene, yellow represents microRNA (miRNA), and pink represents long non-coding RNA (lncRNA).

SNRPB as a risk element for adverse outcomes in multiple cancers, suggesting its potential role in advancing pathological stages and the TNM classification [31]. Corroborating this, our data pinpoints SNRPB as a detrimental factor, aligning with earlier findings. Investigations have demonstrated that SNRPB possibly exerts its effects in tumours via the cell cycle, spliceosome, and p53 signalling pathways [32]. Recent evidence underscores SNRPB's inhibitory influence on the p53 pathway in cervical carcinoma [32]. The specific role of SNRPB in DLBCL remains elusive. Acknowledging DLBCL's intricate mechanism and phenotype landscape, the transition from a normal to malignant state in cells often involves shared functionalities like sustained proliferation [33]. This continuous cell cycle engagement signifies an enduring cell cycle pathway activation. The cell cycle revolves around genetic replication and its consequent distribution to offspring cells [34]. Hence, we postulate that in DLBCL, SNRPB's pathological role might be linked to the cell cycle pathway, a hypothesis that demands in-depth future research.

Centrosomal protein 290 (CEP290) originates from the gene encoding this particular protein. This protein's structure comprises 13 potential coiled-coil domains, six KID motifs, three domains resembling tropomyosin, and a motif consistent with ATP/GTP binding site A [35]. Genetic mutations in CEP290 are linked to conditions such as Joubert syndrome and nephronophthisis. Moreover, antibodies targeting this protein have been tied to multiple cancer types [36, 37]. Through bioinformatic tools and experimental assays, both in vitro and in vivo, our team pinpointed CEP290 as a promising DLBCL prognostic biomarker. Elevated CEP290 expression was more prevalent in tumour samples than in healthy ones. Current data suggests that centrosomal proteins, like CEP, are pivotal in tumour development [36]. For instance, Shan et al. [36] proposed CEP290 as an emerging prognostic metric in liver cancer, influencing cell ferroptosis via the Nrf2 pathway. Shen et al. [38] using bioinformatic approaches, associated CEP290 with papillary thyroid cancer prognosis. Similarly, Yu et al. [39] linked CEP290 to a heightened risk in hereditary nonpolyposis colorectal cancer. Our findings align with the understanding that CEP290 serves as an unfavourable prognostic marker in DLBCL, potentially aiding its progression. To sum up, the potential biomarkers discussed warrant deeper investigative and clinical scrutiny.

Contemporary studies emphasize the distinctiveness of the tumour microenvironment (TME) across lymphoma types, particularly highlighting the inflamed

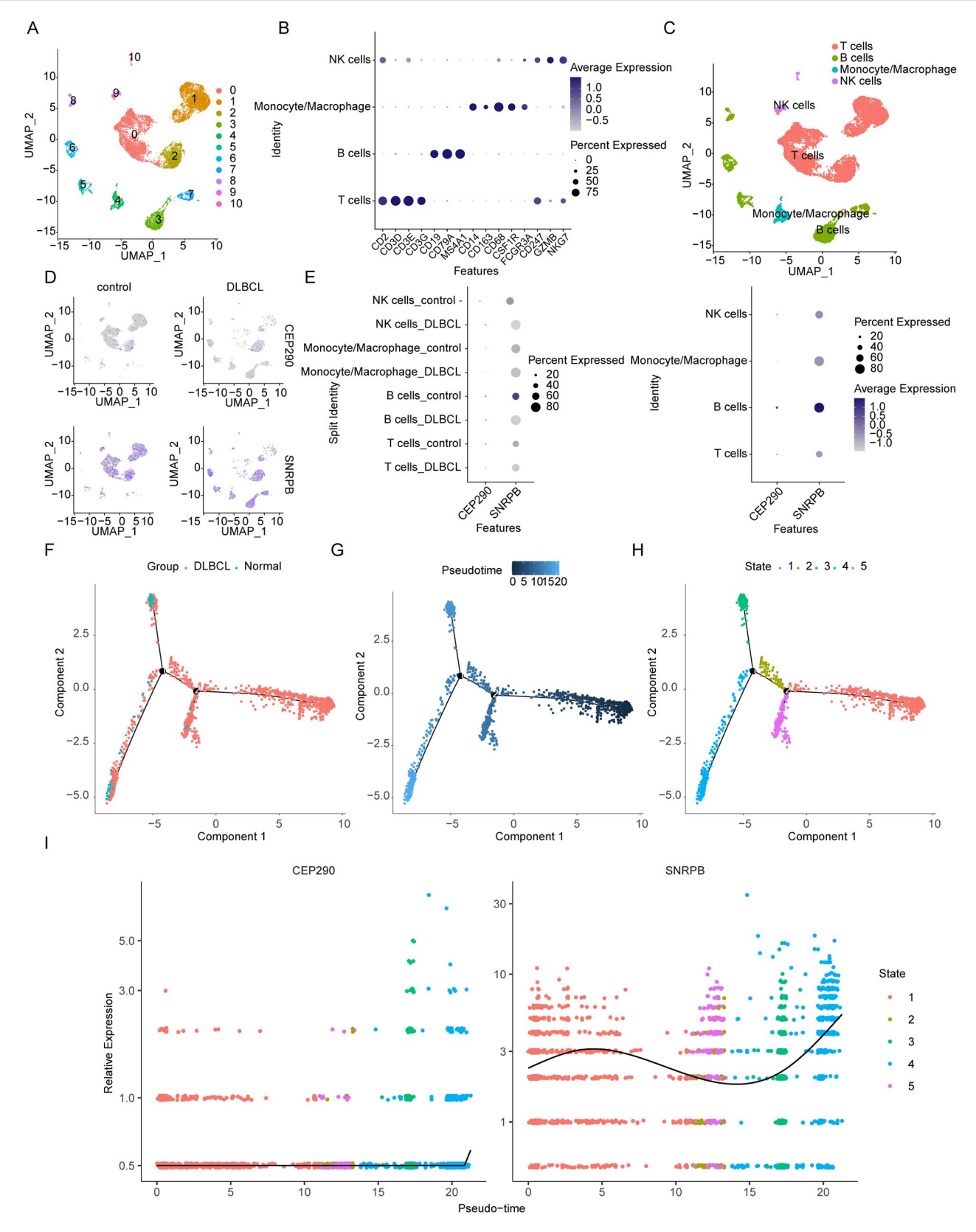


Figure 9. Analysis of single-cell RNA sequencing (scRNA-seq) data in the GSE182434 dataset. (A) Validation of cell clustering results. (B) The dot plot of the expression of marker genes in each cell cluster. (C) The umap clustering plot of the distribution of cell clusters. (D) The distribution of prognostic genes in DLBCL and normal groups. (E) The expression of prognostic genes in different cell clusters in control/DLBCL groups (left) and all samples (right). (F-H) The pseudotime analysis of prognostic genes. F: group; G: time; H: state. (I) The expression of prognostic genes in different branches of B cells.

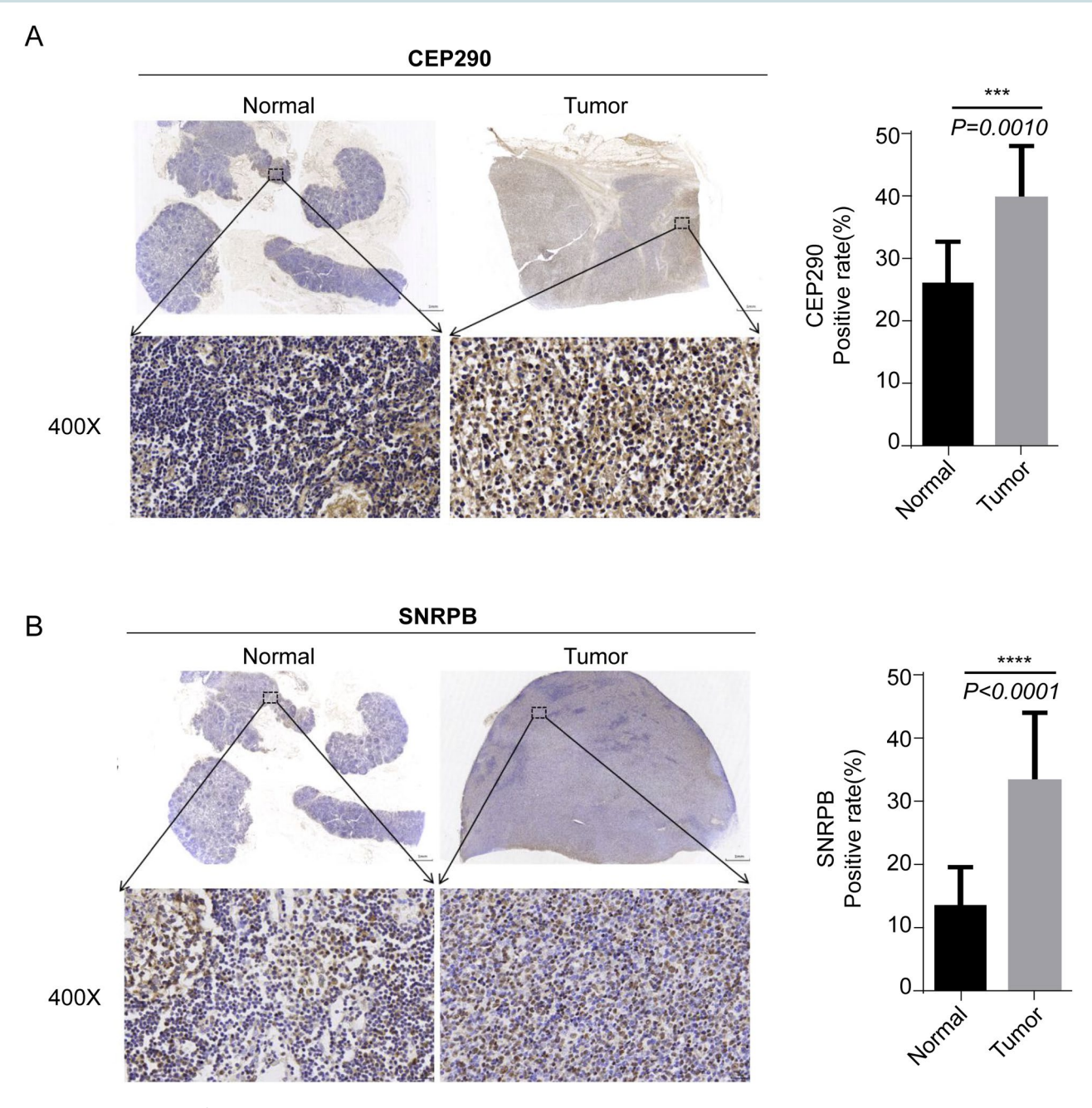


Figure 10. Validation of prognostic genes' expression at protein level. (A) CEP290; (B) SNRPB. ***p < 0.001; ****p < 0.0001.

state present in DLBCL [40]. Insights from Benedetta Apollonio and team [40] underscore the importance of grasping the immune-stroma milieu in DLBCL to refine immunotherapeutic strategies. Based on our immunoassay outcomes, there's a clear positive correlation between SNRPB and naive B cells in DLBCL cases. Past research has illuminated the induction of protein arginine methyltransferase 5 (PRMT5) in naive B cells upon BCR stimulation. This induction augments through B cell receptor signalling, establishing a reciprocal enhancement with PI3K/AKT in lymphoma cells [41]. Such observations suggest SNRPB's potential role in DLBCL progression, possibly by modulating naive B cell expression levels. This avenue might pave the way for fresh perspectives on DLBCL mechanisms. Yang and colleagues [42] devised an immune-centric scoring model, predicated on immune cell infiltration, to forecast DLBCL outcomes, spotlighting the correlation between gamma-delta T cells and patient survival. In our studies, we discerned a positive relationship between CEP290 and gamma-delta T cells in DLBCL. Thus, CEP290 could potentially influence DLBCL's prognosis by modulating gamma-delta T cell dynamics. These findings could enrich our comprehension and drive the genesis of innovative DLBCL therapeutic targets.

The presentation of immune checkpoints on tumour-infiltrating lymphocytes (TILs) can lead to the exhaustion of CD4+ and CD8+T cells, undermining their intrinsic immunocytotoxic capacity and hence, catalyzing tumour progression [43]. Ma et al. [43] postulated that LAG-3 could emerge as a novel immunotherapeutic target. Concurrent administration with PD-1 inhibitors might counteract therapeutic resistance observed in DLBCL patients. Characterized by its 33 kDa weight and 288 amino acid content, CD80 (B7-1) is an immunoglobulin protein stemming from the CD80 gene [44]. Elevated CD80 expression has been documented across various malignancies [45]. The co-stimulatory ligands, CD80(B7-1) and CD86 (B7-2), which originate from antigen-presenting cells (APC), can transmit either augmentative signals through the CD28 receptor or suppressive ones via the CTLA-4 (CD152) receptor [46]. Epigenetic avenues, notably promoter methylation, have been identified as modulators of CD80 and CD86 expression [45]. From Li et al.'s findings [47], CD80 emerged as a recurring target for the miR-30 family, and BCL6's association with ibrutinib resistance in activated B cell-like DLBCL was underscored. In our exploration, we identified pronounced variances in the expression of three immune checkpoint genes: CD276, CD80, and TNFSF4. Specifically, CD276(B7-H3), hailing from the B7 protein family, occupies a pivotal position in cancer dynamics. This immune regulatory protein finds expression selectively in both tumourous and immune cells situated within the TME [48]. Findings by Wang et al. [49] insinuate that cancer stem cells exploit CD276 for immunoevasion, hinting at potential CD276 targeting to diminish CSCs in specific carcinomas. The co-stimulatory checkpoint protein TNFSF4(OX40L), expressed in diverse cell types, has previously been linked to heightened antitumour T-cell activity [50]. Research by Jason Roszik and colleagues [50] correlated diminished TNFSF4 mRNA expression with unfavourable prognosis across melanoma stages. Based on our findings, there's a plausible linkage wherein SNRPB and CEP290 modulate CD276, CD80, and TNFSF4 expressions, subsequently influencing DLBCL progression. The intricate underpinnings of this connection warrant deeper exploration in subsequent investigations.

LncRNAs have established their significance in tumour progression, encompassing initiation, growth, invasion, and metastasis, marking them as promising epigenetic cancer biomarkers and therapeutic candidates [51]. Pivotal roles of microRNAs in physiological pathways, as well as in disease initiation and

progression, particularly across various cancers, have been spotlighted in preceding investigations [52,53]. A specific revelation by Zhao and colleagues [54] highlighted Lnc SMAD5-AS1's capacity to act as a ceRNA, stifling DLBCL proliferation Wnt/β-catenin route. This mechanism operates by sponging miR-135b-5p, augmenting APC expression. In study, Sun et al. [55] pinpointed hsa-miR-513a-5p as a microRNA intricately linked with the onset and evolution of uveal melanoma. Our data linked SNRPB with hsa-miR-513a-5p, leading us to postulate a potential pathway wherein hsa-miR-513a-5p modulates DLBCL progression via SNRPB regulation. Advanced techniques like scRNA-seq have revolutionized our understanding of genetic and transcriptional dynamics within individual cancerous and immune cells across diverse cancers. Utilizing scRNA-seq, Ye and team [56] curated a detailed cellular atlas encompassing both malignant and benign cells in DLBCL. Their insights provide a novel perspective on B cell lymphomagenesis, which could guide targeted immuno-Additionally, our therapy. analyses discerned pronounced SNRPB and CEP290 expressions within B cells, suggesting a conceivable impact of these prognostic markers on B cell-mediated pathways, influencing DLBCL genesis.

In summary, this study pioneers in discerning the prognostic potential of SNRPB and CEP290 within DLBCL. While our findings are promising, this investigation isn't devoid of limitations. Our study was conducted based on a limited number of samples from public databases, and expanding the clinical sample size was a pressing issue. Although we have validated the gene expression by immunohistochemistry, the validation by a large number of cell or animal experiments is still very important. In addition, the validity and applicability of drugs obtained from the analysis need to be verified in the clinical practice. Emphasizing the imperative for deeper experimental mechanistic probes and its translational clinical research, we remain committed to unravelling the mysteries surrounding these genes.

Acknowledgments

Thanks to all authors for their contributions to this manuscript.

Authors contributions

JT, BL, and TB are the principal investigator and conducted statistical analysis and drafted the article. CL, YW, and W-LX performed data management and bioinformatics analysis. JT,

BL, TB, X-JX, CL, YW, and W-LX edited and revised the article. All authors have read and agreed to the published version of the manuscript.

Ethics statement

This study was conducted in accordance with the Declaration of Helsinki, and the data for analysis (GEO database and TCGA-DLBCL dataset) and involving human participants were reviewed and approved by Ethics Committee of Seventh Affiliated Hospital, Sun Yat-Sen University(KY-2024-063-01). Written informed consent to participate in this study was provided by the participants.

Disclosure statement

No potential conflict of interest was reported by the author(s).

Funding

We thank Sanming Project of Medicine in Shenzhen (No. SZSM201911004) and Shenzhen Science and Technology Innovation Commission (JCYJ20230807110659001) for supporting the manuscript preparation and publication.

Data availability statement

The datasets (GSE32018, GSE31312, and GSE182434) were collected from Gene Expression Omnibus (GEO) database (http://www.ncbi.nlm.nih.gov/), and the TCGA-DLBCL dataset was downloaded from The Cancer Genome Atlas (TCGA) database (portal.gdc.cancer.gov). Data supporting the immunohistochemical results of this study are available from the corresponding author (CL) upon reasonable request.

References

- [1] Visco C, Marcheselli L, Mina R, et al. A prognostic model for patients with lymphoma and COVID-19: a multicentre cohort study. Blood Adv. 2022;6(1):327-338. doi: 10.1182/bloodadvances.2021005691.
- [2] Sukswai N, Lyapichev K, Khoury JD, et al. Diffuse large B-cell lymphoma variants: an update. Pathology. 2020;52(1):53-67. doi: 10.1016/j.pathol.2019.08.013.
- [3] Pasqualucci L, Dalla-Favera R. Genetics of diffuse large B-cell lymphoma. Blood. 2018;131(21):2307-2319. doi: 10.1182/blood-2017-11-764332.
- [4] Liu Y, Barta SK. Diffuse large B-cell lymphoma: 2019 update on diagnosis, risk stratification, and treatment. Am J Hematol. 2019;94(5):604–616. doi: 10.1002/ajh.25460.
- [5] Yan J, Yuan W, Zhang J, et al. Identification and validation of a prognostic prediction model in diffuse large B-cell lymphoma. Front Endocrinol (Lausanne). 2022: 13:846357. doi: 10.3389/fendo.2022.846357.
- [6] Pan YB, Wang W, Cai HK, et al. Integrative analysis of a necroptosis-related gene signature of clinical value and heterogeneity in diffuse large B cell lymphoma. Front Genet. 2022;13:911443. doi: 10.3389/fgene.2022.911443.

- [7] Cheng L, Weng B, Jia C, et al. The expression and significance of efferocytosis and immune checkpoint related molecules in pancancer samples and the correlation of their expression with anticancer drug sensitivity. Front Pharmacol. 2022;13:977025. doi: 10.3389/fphar.2022.977025.
- [8] Morioka S, Maueröder C, Ravichandran KS. Living on the edge: efferocytosis at the interface of homeostasis and pathology. Immunity. 2019;50(5):1149-1162. doi: 10.1016/j.immuni.2019.04.018.
- [9] Werfel TA, Cook RS. Efferocytosis in the tumor microenvironment. Semin Immunopathol. 2018;40(6):545-554. doi: 10.1007/s00281-018-0698-5.
- [10] Zhou Y, Yao Y, Deng Y, et al. Regulation of efferocytosis as a novel cancer therapy. Cell Commun Signal. 2020;18(1):71. doi: 10.1186/s12964-020-00542-9.
- [11] Mehrotra P, Ravichandran KS. Drugging the efferocytosis process: concepts and opportunities. Nat Rev Drug Discov. 2022;21(8):601-620. doi: 10.1038/s41573-022-00470-y.
- [12] Trzeciak A, Wang YT, Perry JSA. First we eat, then we do everything else: the dynamic metabolic regulation of efferocytosis. Cell Metab. 2021;33(11):2126-2141. doi: 10.1016/j.cmet.2021.08.001.
- [13] Huang WB, Kuang JF, Li AL, et al. Exploration of short-chain fatty acid-associated hub genes and potential therapeutic targets in primary open-angle glaucoma. Preprint (version 1) available at Research Square. 2024. doi: 10.21203/rs.3.rs-4150868/v1.
- [14] Wilkerson MD, Hayes DN. ConsensusClusterPlus: a class discovery tool with confidence assessments and item tracking. Bioinformatics. 2010;26(12):1572-1573. doi: 10.1093/bioinformatics/btg170.
- [15] He J, Chen Z, Xue Q, et al. Identification of molecular subtypes and a novel prognostic model of diffuse large B-cell lymphoma based on a metabolism-associated gene signature. J Transl Med. 2022;20(1):186. doi: 10.1186/s12967-022-03393-9.
- [16] Colaprico A, Silva TC, Olsen C, et al. TCGAbiolinks: an R/ Bioconductor package for integrative analysis of TCGA data. Nucleic Acids Res. 2016;44(8):e71-e71. doi: 10.1093/ nar/gkv1507.
- [17] Yu G, Wang LG, Han Y, et al. clusterProfiler: an R package for comparing biological themes among gene clusters. OMICS. 2012;16(5):284-287. doi: 10.1089/omi.2011.0118.
- [18] Ritchie ME, Phipson B, Wu D, et al. limma powers differential expression analyses for RNA-sequencing and microarray studies. Nucleic Acids Res. 2015;43(7):e47-e47. doi: 10.1093/nar/gkv007.
- [19] Wang H, Cheng Q, Chang K, et al. Integrated analysis of ferroptosis-related biomarker signatures to improve the diagnosis and prognosis prediction of ovarian cancer. Front Cell Dev Biol. 2021;9:807862. doi: 10.3389/ fcell.2021.807862.
- [20] Shannon P, Markiel A, Ozier O, et al. Cytoscape: a software environment for integrated models of biomolecular interaction networks. Genome Res. 2003;13(11):2498-2504. doi: 10.1101/gr.1239303.
- [21] Stuart T, Butler A, Hoffman P, et al. Comprehensive integration of single-cell data. Cell. 2019;177(7):1888-1902.e21. doi: 10.1016/j.cell.2019.05.031.
- [22] Qiu X, Mao Q, Tang Y, et al. Reversed graph embedding resolves complex single-cell trajectories. Nat Methods. 2017;14(10):979-982. doi: 10.1038/nmeth.4402.

- [23] Ray DM, Morse KM, Hilchey SP, et al. The novel triter-penoid 2-cyano-3,12-dioxooleana-1,9-dien-28-oic acid (CDDO) induces apoptosis of human diffuse large B-cell lymphoma cells through a peroxisome proliferator-activated receptor gamma-independent pathway. Exp Hematol. 2006;34(9):1202–1211. doi: 10.1016/j.exphem. 2006.04.026.
- [24] Leyva-Leyva M, Sandoval A, Felix R, et al. Biochemical and functional interplay between ion channels and the components of the dystrophin-associated glycoprotein complex. J Membr Biol. 2018;251(4):535–550. doi: 10.1007/s00232-018-0036-9.
- [25] Zennaro MC, Boulkroun S, Fernandes-Rosa FL. Pathogenesis and treatment of primary aldosteronism. Nat Rev Endocrinol. 2020;16(10):578–589. doi: 10.1038/ s41574-020-0382-4.
- [26] Lacerda-Abreu MA, Russo-Abrahão T, Meyer-Fernandes JR. The roles of sodium-independent inorganic phosphate transporters in inorganic phosphate homeostasis and in cancer and other diseases. Int J Mol Sci. 2020;21(23):9298. doi: 10.3390/ijms21239298.
- [27] Kanas, G., Ge, W., Quek, R.G.W., Keeven, K., Nersesyan, K., and Jon, E.A. (2022). Epidemiology of diffuse large B-cell lymphoma (DLBCL) and follicular lymphoma (FL) in the United States and Western Europe: population-level projections for 2020–2025. Leukemia Lymphoma 63(1), 54–63. doi: 10.1080/10428194.2021.1975188.
- [28] Doran AC, Yurdagul A, Jr., Tabas I. Efferocytosis in health and disease. Nat Rev Immunol. 2020;20(4):254–267. doi: 10.1038/s41577-019-0240-6.
- [29] Tajbakhsh A, Gheibihayat SM, Taheri RA, et al. Potential diagnostic and prognostic of efferocytosis-related unwanted soluble receptors/ligands as new non-invasive biomarkers in disorders: a review. Mol Biol Rep. 2022;49(6):5133–5152. doi: 10.1007/s11033-022-07224-4.
- [30] Sun D, Ou YC, Hoch SO. Analysis of genes for human sn-RNP Sm-D1 protein and identification of the promoter sequence which shows segmental homology to the promoters of Sm-E and U1 snRNA genes. Gene. 1997; 189(2):245–254. doi: 10.1016/s0378-1119(96)00858-x.
- [31] Wu J, Lu F, Yu B, et al. The oncogenic role of SNRPB in human tumors: a pan-cancer analysis. Front Mol Biosci. 2022;9:994440. doi: 10.3389/fmolb.2022.994440.
- [32] Zhu L, Zhang X, Sun Z. SNRPB promotes cervical cancer progression through repressing p53 expression. Biomed Pharmacother. 2020;125:109948. doi: 10.1016/j.biopha. 2020.109948.
- [33] Hanahan D. Hallmarks of cancer: new dimensions. Cancer Discov. 2022;12(1):31–46. doi: 10.1158/2159-8290. Cd-21-1059.
- [34] Zou T, Lin Z. The involvement of ubiquitination machinery in cell cycle regulation and cancer progression. Int J Mol Sci. 2021;22(11):5754. doi: 10.3390/ijms22115754.
- [35] Moradi P, Davies WL, Mackay DS, et al. Focus on molecules: centrosomal protein 290 (CEP290). Exp Eye Res. 2011;92(5):316–317. doi: 10.1016/j.exer.2010.05.009.
- [36] Shan Y, Yang G, Lu Q, et al. Centrosomal protein 290 is a novel prognostic indicator that modulates liver cancer cell ferroptosis via the Nrf2 pathway. Aging (Albany NY). 2022;14(5):2367–2382. doi: 10.18632/aginq.203946.
- [37] Wang L, Yang Y, Song J, et al. Two novel mutations in the C-terminal region of centrosomal protein 290 (CEP290)

- result in classic Joubert syndrome. J Child Neurol. 2015;30(6):772–776. doi: 10.1177/0883073814535488.
- [38] Shen Y, He W, Wang D, et al. Identification of gene coexpression modules and prognostic genes associated with papillary thyroid cancer. J Oncol. 2022;2022: 9025198–9025114. doi: 10.1155/2022/9025198.
- [39] Yu L, Yin B, Qu K, et al. Screening for susceptibility genes in hereditary non-polyposis colorectal cancer. Oncol Lett. 2018;15(6):9413–9419. doi: 10.3892/ol. 2018.8504.
- [40] Apollonio B, Ioannou N, Papazoglou D, et al. Understanding the immune-stroma microenvironment in B cell malignancies for effective immunotherapy. Front Oncol. 2021;11:626818. doi: 10.3389/fonc.2021.626818.
- [41] Zhu F, Guo H, Bates PD, et al. PRMT5 is upregulated by B-cell receptor signaling and forms a positive-feedback loop with PI3K/AKT in lymphoma cells. Leukemia. 2019;33(12):2898–2911. doi: 10.1038/s41375-019-0489-6.
- [42] Yang J, Yu L, Man J, et al. Immune scoring model based on immune cell infiltration to predict prognosis in diffuse large B-cell lymphoma. Cancer. 2023;129(2):235–244. doi: 10.1002/cncr.34519.
- [43] Ma J, Pang X, Li J, et al. The immune checkpoint expression in the tumor immune microenvironment of DLBCL: clinicopathologic features and prognosis. Front Oncol. 2022;12:1069378. doi: 10.3389/fonc.2022.1069378.
- [44] Golubovskaya V. CAR-T cells targeting immune checkpoint pathway players. Front Biosci (Landmark Ed). 2022;27(4):121. doi: 10.31083/j.fbl2704121.
- [45] de Vos L, Grünwald I, Bawden EG, et al. The landscape of CD28, CD80, CD86, CTLA4, and ICOS DNA methylation in head and neck squamous cell carcinomas. Epigenetics. 2020;15(11):1195–1212. doi: 10.1080/15592294.2020. 1754675.
- [46] Harding FA, McArthur JG, Gross JA, et al. CD28-mediated signalling co-stimulates murine T cells and prevents induction of anergy in T-cell clones. Nature. 1992;356 (6370):607–609. doi: 10.1038/356607a0.
- [47] Xu P-P, Sun C, Cao X, et al. Immune characteristics of Chinese diffuse large B-cell lymphoma patients: implications for cancer immunotherapies. EBioMedicine. 2018;33:94–104. doi: 10.1016/j.ebiom.2018.06.010.
- [48] Getu AA, Tigabu A, Zhou M, et al. New frontiers in immune checkpoint B7-H3 (CD276) research and drug development. Mol Cancer. 2023;22(1):43. doi: 10.1186/s12943-023-01751-9.
- [49] Wang C, Li Y, Jia L, et al. CD276 expression enables squamous cell carcinoma stem cells to evade immune surveillance. Cell Stem Cell. 2021;28(9):1597–1613.e7. doi: 10.1016/j.stem.2021.04.011.
- [50] Roszik J, Markovits E, Dobosz P, et al. TNFSF4 (OX40L) expression and survival in locally advanced and metastatic melanoma. Cancer Immunol Immunother. 2019;68(9):1493–1500. doi: 10.1007/s00262-019-02382-0.
- [51] Meseure D, Drak Alsibai K, Nicolas A, et al. Long non-coding RNAs as new architects in cancer epigenetics, prognostic biomarkers, and potential therapeutic targets. Biomed Res Int. 2015;2015:320214–320214. doi: 10.1155/2015/320214.
- [52] Zhuang H, Ma Z, Huang K, et al. Establishment of a 7-miRNA-based risk score system for predicting

- prognosis of pancreatic cancer. Pancreas. 2020;49(5):655-662. doi: 10.1097/mpa.000000000001542.
- [53] Wang Q, Xu K, Tong Y, et al. Novel miRNA markers for the diagnosis and prognosis of endometrial cancer. J Cell Mol Med. 2020;24(8):4533-4546. doi: 10.1111/ jcmm.15111.
- [54] Zhao C, Jiao C, Zhang Y, et al. Lnc SMAD5-AS1 as ceRNA inhibit proliferation of diffuse large B cell lymphoma via Wnt/β-catenin pathway by sponging
- miR-135b-5p to elevate expression of APC. Cell Death Dis. 2019;10(4):252. doi: 10.1038/s41419-019-1479-3.
- [55] Sun Y, Zhang X, Cong Z, et al. Identification of 5 microR-NA biomarkers associated with the prognosis of uveal melanoma. Medicine (Baltimore). 2022;101(35):e30366. doi: 10.1097/md.0000000000030366.
- [56] Ye X, Wang L, Nie M, et al. A single-cell atlas of diffuse large B cell lymphoma. Cell Rep. 2022;39(3):110713. doi: 10.1016/j.celrep.2022.110713.